JOURNAL OF GEOPHYSICAL RESEARCH, VOL. 96, NO. A9, PAGES 15,801-15,810, SEPTEMBER 1, 1991

THE EVOLUTION OF FIELD-ALIGNED CURRENTS AS A FUNCTION OF SUBSTORM PHASE

Francis K. Chun and Christopher T. Russell

Institute of Geophysics and Planetary Physics and Department of Earth and Space Sciences, University of California, Los Angeles

Abstract. ISEE 1 and 2 measurements of magnetic changes across nightside field-aligned currents at mid altitudes in the inner magnetosphere are examined to determine the average ionospheric extrapolated characteristics and properties of region 1 and 2 currents as a function of substorm phase. The properties of these currents studied include current intensity, density, layer width, and velocity and are consistent with earlier studies at lower altitudes. In general, region 1 and 2 currents behave differently during substorm growth and expansion, but are comparable in the recovery phase. During a substorm, region 1 current intensity ranges from 0.4 to 0.6 A/m and peaks during the expansion phase. Region 2 intensity varies from 0.15 to 0.35 A/m and reaches a maximum during recovery. The density of region 2 currents remains essentially steady at 1.4 $\mu A/m^2$, while region 1 decreases from 5 to 1.3 $\mu A/m^2$. The width of these current sheets throughout a substorm remains in the range from 100 to 500 km. The velocity of these sheets is for the most part inwards with speeds from 50 to 200 m/s. Even though these current sheet crossings were not originally selected as substorm associated events, they all occurred during one of the phases of a substorm. This indicates that substorms play a major role in the generation of nightside region 1 and 2 currents detected by the ISEE spacecraft. These results are consistent with a model in which these currents flow to couple the outer magnetosphere and the ionosphere in response to the stresses applied by both dayside and nightside reconnection. Region 1 currents are responsive to variations in the stress caused by both reconnection regions, whereas region 2 currents are responsive to only nightside reconnection.

Introduction

Field-aligned currents play a major role in the magnetosphere-ionosphere interaction transporting stress from one region to the other. Consequently, this type of current system is an integral part of the global system of currents. The two large-scale field-aligned current structures that connect the outer magnetosphere to the auroral ionosphere have been called region 1 and region 2 currents [*Iijima and Potemra*, 1976]. Region 1 currents flow into the ionosphere on the dawn side and out of the ionosphere on the duskside, while region 2 is in the opposite sense with outward flow on the dawnside and inward flow on the duskside. The region 1 currents lie poleward of the region 2 currents. For the most part, these currents are always present except during extended periods of very low geomagnetic activity. During periods when the interplanetary magnetic field is zero or northward, the large-scale region 1 and region 2 current system diminish substantially near midnight, whereas the currents at other local times, especially the cleft currents near noon, continue without change [*Rich and Gussenhoven*, 1987].

In the past, region 1 and region 2 currents have been correlated with geomagnetic activity and interplanetary magnetic field (IMF) orientation [*Iijima and Potemra*, 1976], as well as with substorms [*Iijima and Potemra*, 1978]. *Akasofu* [1964] proposed that auroral substorms occurred in two phases, the expansive phase and the recovery phase. However, as the understanding of substorms and their related processes grew, it became evident that many auroral phenomena in isolated substorms occurred prior to the onset of the expansive phase. This phase was termed the growth phase [*McPherron*, 1970]. We now understand the growth phase as the period during which energy is stored in the magnetotail. The expansion phase is the period in which explosive energy release begins in the magnetotail, and the recovery phase signifies the relaxation of the magnetosphere from its previous stressed state. A more modern definition of the overall substorm process is "...a transient process initiated on the night side of the earth in which a significant amount of energy derived from the solar wind-magnetosphere interaction is deposited in the auroral ionosphere and magnetosphere [*McPherron*, p.657, 1979]." Field-aligned currents play a major role in helping this energy deposition and relieving the magnetosphere of its internal stresses.

In this paper we address the determination of the average properties and characteristics of large-scale nightside region 1 and region 2 currents in each phase of a substorm. Are region 1 and 2 currents associated at all with substorms and consequently, a substorm phase? Do these currents develop differently or similarily as the substorm progresses? How does the width of the current layers change from one phase to another? Do these current systems move and if so, how does the velocity of these current structures change in the course of a substorm? These are just a few of the questions we attempt to answer in examining the effects substorm phase has on region 1 and region 2 currents.

In their 1978 paper, Iijima and Potemra presented statistical characteristics of region 1 and region 2 currents during various phases of substorms and at various magnetic local times using low-altitude magnetometer data from the Triad satellite. Their work was extensive and yielded results on the intensities, densities, and

Paper number 91JA01018.
0148-0227/91/91JA-01018$05.00

relative strengths of region 1 and region 2 currents during the different substorm phases and substorm activity level. As we will show below, the ISEE 1 and 2 measurements at mid altitudes in the magnetosphere are consistent with these earlier results at low altitudes indicating that ISEE is indeed observing the same current systems.

In this paper we examine field-aligned currents calculated from mid altitude nightside magnetic field measurements made by ISEE 1 and 2 in the inner magnetosphere between 2.4 to 7 R_E, using a set of observations first compiled by *Kelly et al.* [1986]. In addition to intensity, density and thickness measurements of the current structures, Kelly et al.'s study has been the only one to measure the velocity of the current structure. We divide our substorms into the three classic phases (growth, expansion, and recovery) discussed above. Iijima and Potemra divided their substorm into four phases (quiet, expansion, recovery, and weak disturbance), but as we discuss below all our events fall in the three classic phases.

We begin our examination with a brief description of the data base along with a discussion on how we extrapolated these quantities to the ionosphere. We then describe our method of determining substorm phases for each field-aligned current event and then present our results. We finish with a discussion on the implications of our study and conclusions from this work. For the ease of comparison with earlier studies the Kelly et al. terms of surface current density (current/length) and average current density (current/area) are referred herein as current intensity and current density, respectively.

Description of Database

Kelly et al. used ISEE 1 and 2 magnetometer data from their first 180 orbits covering a time period from October 1977 to December 1978. Out of those orbits, they identified 27 clear events of large-scale field-aligned currents. These events were found in the inner magnetosphere between 2.4 to 7 R_E and on the late afternoon and nightside between the local times of 1530 to 0545 hours. To identify these field-aligned currents, Kelly et al. first transformed the ISEE magnetic field data into a dipole coordinate system, or field-aligned system, and then subtracted a model field from the observed field leaving only the variations from the average field. If field-aligned currents are sheetlike, their magnetic signatures will be in one of the transverse directions. Figure 1 is a plot from Kelly et al.'s study showing a sample of the detrended data for one of their events. The magnetic perturbation due to a field-aligned sheet like structure can be seen in the B_y component under the shaded region labeled "b".

The net monotonic change in B_y under this "b" region is around 32 nT. From Ampere's law this corresponds to a current intensity of 25.6 mA/m. The current sheet velocity can then be determined by knowing the mean spacecraft separation, the mean time delay between ISEE 1 and 2 observations, and the spacecraft velocity. Multiplying the current sheet velocity by the duration of the observed signature yields an estimate of the current layer width. Knowing the current layer width, the current density in nA/m^2 can be calculated. Finally, Kelly et al. then determined

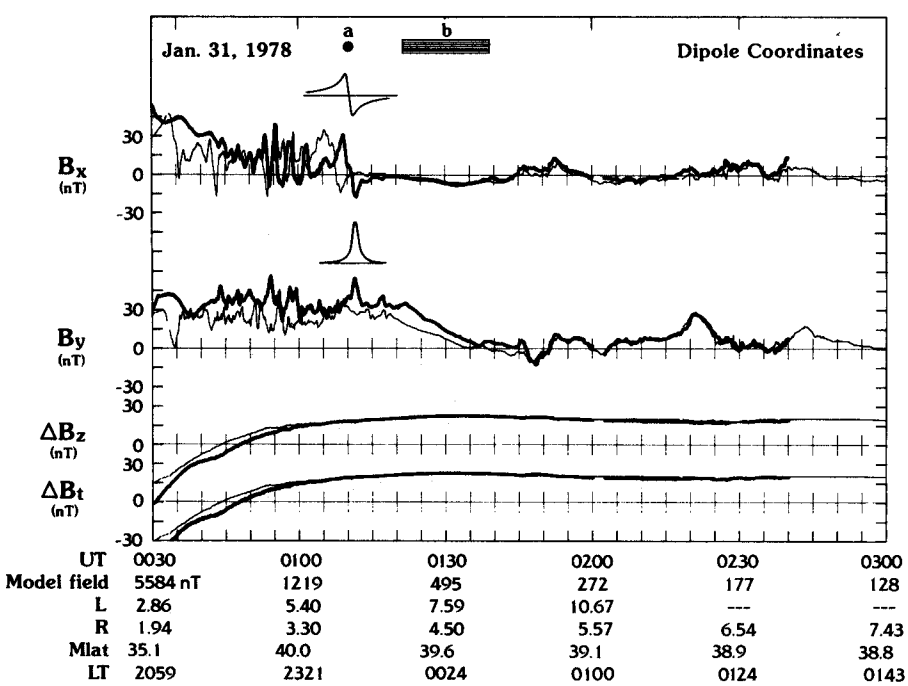

Fig. 1. Sample magnetic time series of ISEE 1 and 2 detrended data for January 31, 1978 (Event 5) taken from *Kelly et. al.*, [1986]. ISEE 1 data are shown by the heavy trace, and ISEE 2 by the thin trace. The magnetic perturbation due to a field-aligned current sheet can be seen in the B_y component under the shaded region labeled "b".

whether the field-aligned current event was a region 1 sense current, region 2 sense current, or a small-scale current structure based on the event's local time and direction of current flow (i.e., current flow into the ionosphere or out of the ionosphere).

In addition to magnetic field measurements, Kelly et al. examined plasma particle data from three ISEE plasma experiments; the Los Alamos/Garching Fast Plasma Experiment, the University of California, Berkeley, medium-energy solid state telescopes, and the Los Alamos medium-energy particle instruments. We will not repeat this discussion here. We refer the reader to Kelly et al. for the discussion of the plasma observations associated with these currents.

A summary of the field-aligned current properties can be found in Tables 1 and 2 of Kelly et al.'s paper. The observations listed in these tables were made at a variety of magnetic latitudes and distances within the inner magnetosphere. To remove any effects due to the variations in the location of the observations, we normalized each observation to an altitude of 100 km in the ionosphere. Table 1 in our paper lists the various currents classified according to the direction of the current (region 1 or region 2 current) and substorm phase. The average ionospheric values for current intensity, density, layer width, and velocity are also included.

Extrapolation of Properties to Ionosphere

In this paper we will define field-aligned current intensity as the current flowing in the current sheet per unit length, along the sheet perpendicular to the current and the magnetic field. We define the term current density to be the current intensity divided by the thickness of the current layer, perpendicular to the current sheet. To map the current intensity measured at some location along a field line in the inner magnetosphere to a location within the ionosphere, we must determine how the width of the current sheet (in the direction perpendicular to the field) varies with magnetic latitude. Figure 2 shows a diagram illustrating this relationship. $J_{intensity}$ is inversely proportional to the width, δS. Looking at the top view of Figure 2, as δS decreases, from l_1 to l_2, $J_{intensity}$ increases. The lengths, l_2 and l_1, are the perpendicular distance to the Earth's dipole axis and are related to the magnetic colatitude and radial distance by $l=R\sin\theta$ (see side view, Figure 2). Since for any dipole field line, $R=L\sin^2\theta$, where L is the L shell value of that field line,

$$J_{intensity} \propto \frac{1}{\sin^3\theta} \quad (1)$$

where θ is the magnetic colatitude.

To map the current density along the magnetic field, consider a field-aligned current sheet structure with a finite cross-sectional area in the equatorial plane. If we move along this flux tube to a lower altitude, the magnetic flux will be conserved as well as total current. Magnetic flux associated with this structure is given by

$$\phi_{open\ surface} = \int B \cdot dA = const$$

or for a uniform magnetic field,

$$B \times A = const$$

where B is the magnetic field strength and A is the cross-sectional area. If total field-aligned current is conserved, then

$$J \propto B \quad (2)$$

TABLE 1. Substorm Phase Breakdown of Region 1 and 2 Ionospheric Current Properties

Region	Substorm Phase	Event	Current Intensity, A/m		Current Density, μA/m²		Cur Layer Width, km		Current Sheet Vel, m/sec	
			Estimate	Average	Estimate	Average	Estimate	Average	Estimate	Average
1	gro	11	0.414	0.388	0.417	4.979	993	516	-288	-164
		26	0.362		9.540		38		-39	
1	exp	13	0.398		0.521		763		-48	
		20	0.727	0.630		2.391		471		-53
		24	0.764		4.260		179		-57	
1	rec	5	0.225		0.625		360		-164	
		15	0.179		0.627		285		-140	
		18	0.375	0.360	1.051	1.283	357	290	-199	-65
		22	0.449		2.828		159		-37	
		28	0.574							
2	gro	6	0.206	0.151	2.077	1.318	99	135	-48	-63
		8	0.095		0.559		170		-78	
2	exp	7	0.269		2.293		117		-256	
		12	0.414		0.673		616		-236	
		19	0.428	0.339	2.538	1.551	169	346	-123	-190
		23	0.337		0.700		482		-146	
		27	0.248							
2	rec	14	0.288		1.256		229		-16	
		17	0.458	0.354	1.248	1.252	367	298	-98	-57
		21	0.317							
2	rec	14	0.288		1.256		229		-16	
		17	0.458	0.354	1.248	1.252	367	298	-98	-57
		21	0.317							

Extrapolation of Current Intensity

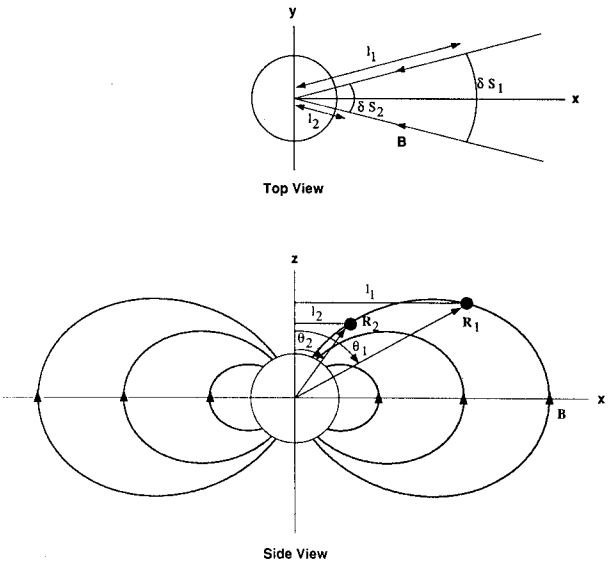

Fig. 2. This diagram illustrates the extrapolation of current intensity to the ionosphere. The top view shows how current intensity is inversely proportional to the arc length δS. As δS decreases from 1 to 2, current intensity will increase. The side view shows how to relate arc length, and thus intensity, to magnetic colatitude.

Since the magnetic field strength B, due to a dipole field, is given by

$$B = \frac{B_o}{R^3}\sqrt{4\cos^2\theta + \sin^2\theta}$$

and since

$$R = L \sin^2\theta$$

where R is the radial distance in R_E, B_o is the equatorial surface field strength, θ is the magnetic colatitude, and L is the L value, we find that

$$J \propto \frac{1}{\sin^6\theta}\sqrt{4 - 3\sin^2\theta} \qquad (3)$$

The current layer thickness can be found by dividing current intensity by current density.

To extrapolate the current sheet velocity, we assume that the entire current sheet structure moves as a unit, mapping to a new dipole field line and a new invariant latitude. We illustrate this extrapolation in Figure 3, which is a diagram of a dipole field along with the equipotential of the field. We use an orthogonal dipole coordinate system developed by *Cummings et al.* [1969], where the curves of constant υ are the dipole field lines and the curves of constant μ are the equipotentials. The unit vector $\mathbf{e}_\mu$ is parallel to the field line; $\mathbf{e}_\upsilon$ is parallel to the equipotential; and $\mathbf{e}_\phi$ is in the azimuthal direction to complete the system. The coordinates of any point in this field are then represented by, υ, μ, and ϕ, where υ is constant along a field line, μ is constant along an equipotential,

Extrapolation of Current Sheet Velocity

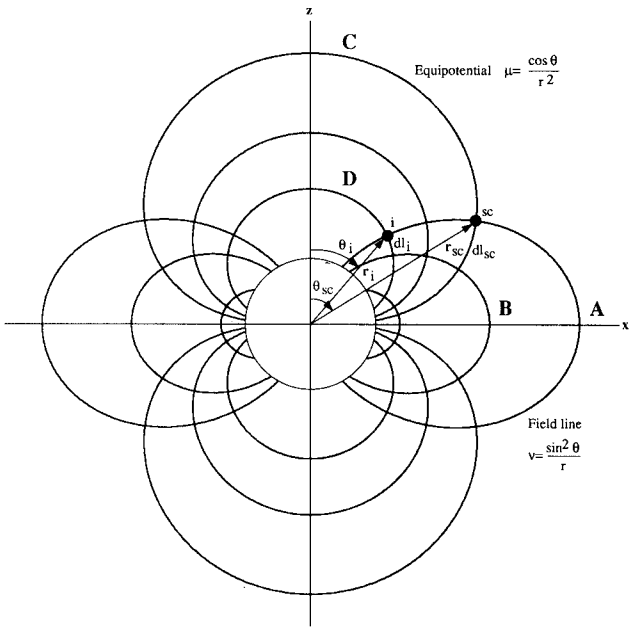

Fig. 3. Dipole field with equipotentials illustrating the extrapolation of current sheet velocity to the ionosphere. Spacecraft measurements of the sheet velocity made at the point sc can be extrapolated to the ionosphere i by using a dipole coordinate system devised by *Cummings et al.*, [1969]. In this coordinate system, υ is constant along a field line and μ is constant along equipotentials.

and ϕ is the ordinary azimuthal spherical coordinate. The variables υ and μ are given by the following equations:

$$\nu = \frac{\sin^2\theta}{r} \qquad (4)$$

$$\mu = \frac{\cos\theta}{r^2} \qquad (5)$$

where r and θ are the radial distance and dipole colatitude as shown in the figure.

We take our observed field-aligned current structure to lie along field line "*A*." The velocity of that current structure is in a direction along the corresponding equipotential "*C*," which intersects the field line "*A*" at point "*sc*" (for spacecraft position). If we assume that the entire dipolar current sheet moves as a unit, then after some time interval δt the entire structure will move from field line "*A*" to field line "*B*." The velocities at the two locations "*sc*" and "*i*" (for ionosphere) will be related to the distances (dl_{sc} and dl_i) between field lines "*A*" and "*B*" as measured along their corresponding equipotentials "*C*" and "*D*." The ratios of the velocities of the current sheet at "sc" and "i" are given by

$$\frac{v_i}{v_{sc}} = \frac{dl_{sc}/dt}{dl_i/dt} = \frac{dl_{sc}}{dl_i} \qquad (6)$$

In spherical coordinates the length dl along the equipotential or line of constant μ is given by

$$dl = \sqrt{(dr)^2 + (rd\theta)^2}|_\mu \quad (7)$$

where $|_\mu$ indicates that this length is measured along an equipotential. We can rewrite (7) as

$$dl = \frac{\partial\theta}{\partial v} dv \sqrt{\left(\frac{dr}{d\theta}\right)^2 + r^2}|_\mu \quad (8)$$

where $\partial\theta/\partial v$ is found from (4) and (5). After some manipulation it can be shown that

$$dl = \frac{\sin^3\theta}{v(1 + 3\cos^2\theta)} \sqrt{4\sin\theta + \cos^2\theta} \quad (9)$$

Therefore, to find v_i, we evaluate (9) for the spacecraft location and a location in the ionosphere and substitute them into (6).

Figure 4 illustrates the functional relationships, equations (1), (3) and (9), for the extrapolation of current intensity, current density, and current sheet velocity as a function of magnetic latitude. As latitude increases, intensity and density increase and velocity decreases. The greatest change occurs in the density profile while the smallest change occurs in intensity.

Determination of Substorm Phase

To determine the substorm phase of our various events, we examined plots of magnetic indices *AU*, *AL*, *AE*, and *AO*, digital ground station magnetometer data and analog ground station magnetograms. The magnetic indices data were obtained from the WDC-C2 for Geomagnetism Data Book compiled by *Kamei* and *Maeda* [1981]. The digital ground station data are those obtained during the International Magnetospheric Study on magnetic tapes. This data set includes data from many of the North American auroral stations, various low-latitude stations and several Scandinavian stations. The analog ground station magnetograms are stored as microfiche here and includes stations worldwide.

The AE (auroral electrojet) indices, which includes *AU*, *AL*, *AE*, and *AO*, was developed by *Davis* and *Sugiura* in [1966] as a global measure of the geomagnetic auroral electrojet activity level. The *AE* indices are derived from the horizontal, or *H* component of 10-13 northern hemisphere auroral zone magnetic observatories. *AU* is given by the largest value from any of the stations and is a measure of the eastward electrojet current intensity. *AL* is the smallest value from any station and measures the intensity of the westward electrojet. *AE* is the difference between *AU* and *AL* and is a measure of the overall activity of the electrojets, while *AO* is the mean value of *AU* and *AL* and is regarded as a measure of the equivalent zonal current [*Kamei and Maeda*, 1981]. Figure 5 is a 24-hour plot of the *AE* indices for March 15, 1978, with the phases of the substorm shown. Field-aligned current events 19 and 20 occur between 0115 to 0127 UT during the expansion phase of the substorm.

We can also determine the phase of a substorm by examining magnetometer (digital and analog) data from various stations located in the auroral zone. For each event we examined data from those stations near geographic midnight. If a substorm occurred near the time of any of our field-aligned current events, then we should observe the magnetic signature of that substorm as a depression in the H component.

Figure 6 is a 6-hour time series plot of digital magnetometer data from three Scandinavian stations; Skarsvag, Kunes, and Kevo. These

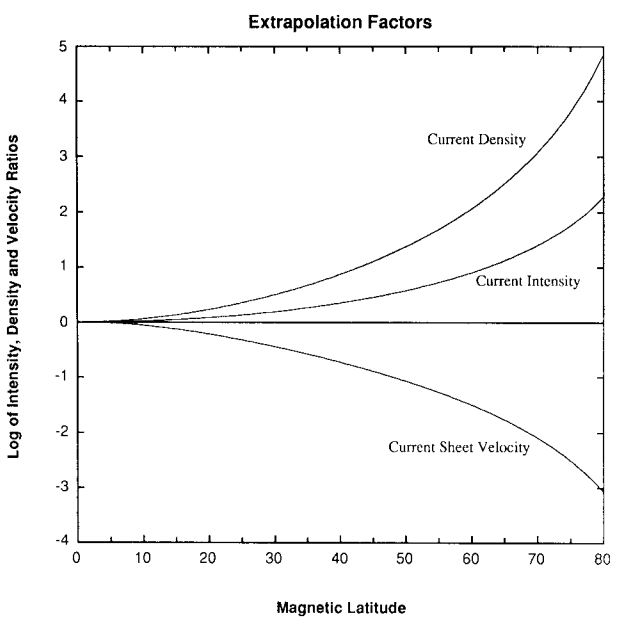

Fig. 4. Extrapolation factors for current intensity, density, and sheet velocity calculated from equations (1), (3), and (9). The log of each parameter with respect to its equatorial value is plotted versus magnetic latitude. Intensity and density increase with latitude, while velocity decreases. The greatest change is in density and the smallest change is in intensity.

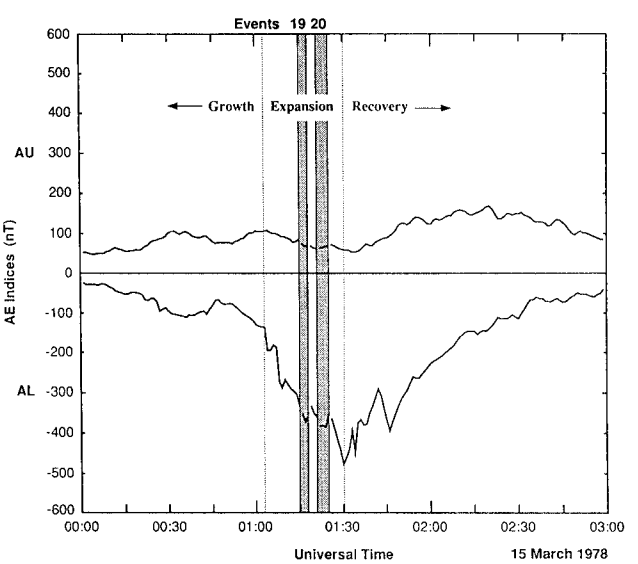

Fig. 5. Time series of AU and AL indices for events 19 and 20, March 15, 1978, with substorm phases depicted. Both events occur during the expansion phase.

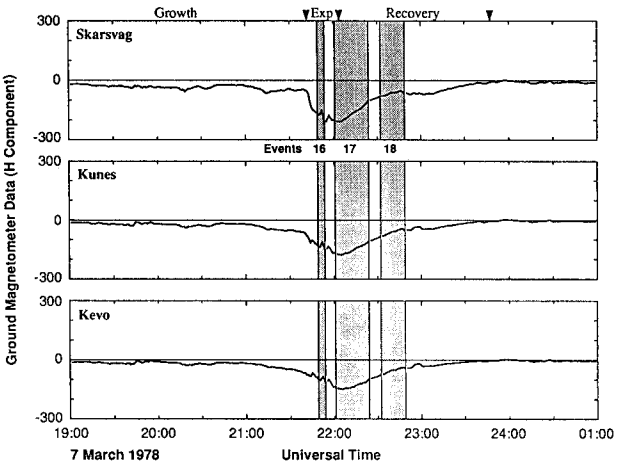

Fig. 6. Time series of the H component of digital ground station magnetic data, with substorm phases depicted, for events 16, 17, and 18, March 7, 1978. The data is from three Scandinavian stations, Skarsvag, Kunes and Kevo. Event 16 occurs during the expansion phase, while events 17 and 18 occurs in recovery.

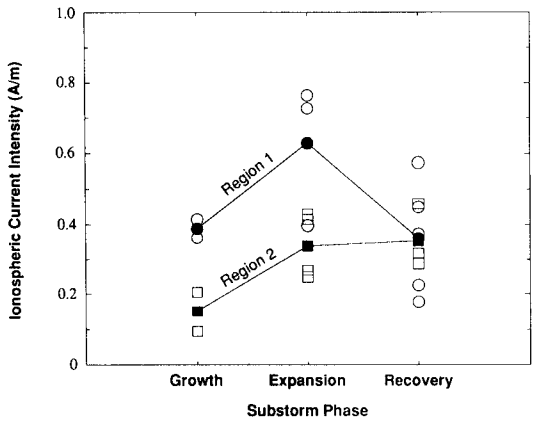

Fig. 7. Ionospheric region 1 and 2 current intensity (A/m) versus substorm phase. The open circles are estimates of the region 1 intensity given in Table 1, while the open boxes represent region 2. The average values of region 1 and region 2 intensities during each phase are shown as the connected dark circles and boxes, respectively.

stations range in geomagnetic latitude from 68° to 66° and were located around geographic midnight for our March 7, 1978 (2149-2249 UT) events. Skarsvag detected a substorm with three very clear phases. The other two stations appear to be too far south of the substorm onset region to clearly separate the growth and expansion phases. Onset occurred around 2140 UT or possible slightly earlier. Since Skarsvag is our highest-latitude station at this time, it is possible that the substorm could have been detected a few minutes earlier further north. The first March 7 event therefore occurred after the onset of the expansion phase and the last two events occurred in the recovery phase. We were able to determine the substorm phase for every event, except the first four which occurred in late 1977, and for which insufficient ground station data and magnetic indices data were available at the time of our study. The substorm phases for all of the events are listed in Table 1.

Results

Once the substorm phase was determined for each event, we binned the various estimated ionospheric field-aligned current properties according to whether they were region 1 or region 2 sense currents and according to substorm phase. We then calculated the averages for each of the six bins of the various ionospheric field-aligned current parameters and plotted those averages and the appropriate current properties versus substorm phase. Figures 7-10 show the various ionospheric field-aligned current parameters as a function of substorm phase. The individual region 1 and region 2 events are plotted as open circles and boxes, respectively, while the average values are the dark circles and boxes connected by lines.

Figure 7 shows region 1 and region 2 current intensity as a function of substorm phase. The interesting feature of Figure 7 is the distinct difference between the evolution of region 1 and

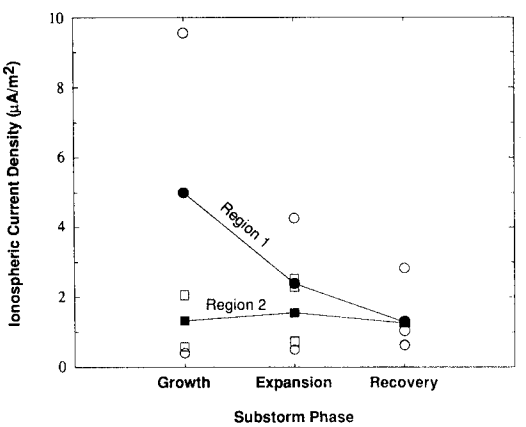

Fig. 8. Ionospheric region 1 and 2 current density ($\mu A/m^2$) versus substorm phase. The format is the same as Figure 7.

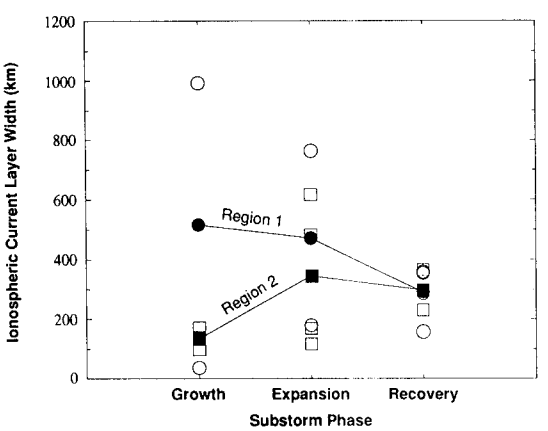

Fig. 9. Ionospheric region 1 and 2 current layer width (km) versus substorm phase. The format is the same as Figure 7.

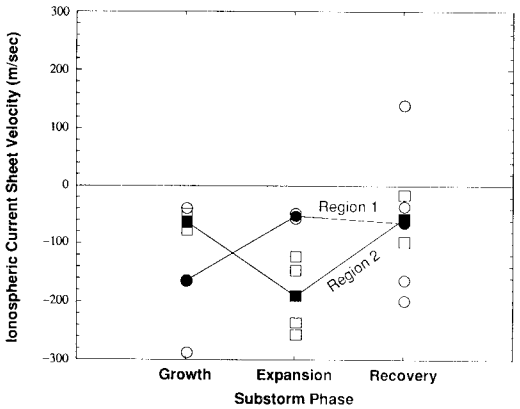

Fig. 10. Ionospheric region 1 and 2 current sheet velocity (m/sec) versus substorm phase. The format is the same as Figure 7.

2 intensities. Region 1 experiences a definite peak in the expansion phase, while region 2 does not. In general, region 1 intensity is greater than region 2 intensity throughout a substorm except during the recovery phase. Region 1 intensity starts around 0.39 A/m in the growth phase, increases to a maximum of 0.63 A/m in expansion, and then decreases to growth phase levels of around 0.36 A/m during recovery. Region 2 intensity, however, is about 0.15 A/m during the growth phase, increases to 0.34 A/m in expansion, and then increases again very slightly to 0.35 A/m in recovery. Region 1 intensity is on the order of 2.6 times that of region 2 during the growth phase and around 1.9 times greater during expansion. *Iijima and Potemra* [1978] reported comparable ratios of region 1 and 2 intensities in the afternoon to midnight sectors. However, in their report, instead of distinguishing between substorm phase, Iijima and Potemra distinguished between geomagnetic activity level; $|AL| < 100\gamma$ and $|AL| \geq 100\gamma$. For purposes of comparisons, we will associate $|AL| < 100\gamma$ with the growth phase, and $|AL| \geq 100\gamma$ with the expansion phase. We will also concentrate our comparison with their afternoon to midnight sector averages since most of our events occur in that local time interval. In this sector they found region 1 to 2 intensity ratios for these two activity levels on the order of 2.4 and 1.8. Region 1 intensity increases by a factor of 1.6 from the growth to the expansion phase, whereas region 2 increases by 2.2. This too, compares favorably to Iijima and Potemra's results. In the afternoon to midnight sector they found that region 1 increased by a factor of 1.7 from $|AL| < 100\gamma$ to $|AL| \geq 100\gamma$, while region 2 increased by 2.2.

Figure 8 is a plot of region 1 and 2 current density with substorm phase. Data are limited to two events each for the region 1 growth phase and expansion phase, which have large variances with respect to their averages possibly because these phases are dynamic times and possibly due to substorm-to-substorm variations. The resulting average value shown is of course highly uncertain. However, region 1 and 2 appear to behave differently during a substorm. Region 1 density continuously decreases throughout a substorm, whereas region 2 remains steady with a very slight peak during expansion. As in intensity, region 1 density appears to be greater than region 2 density during all phases of a substorm except the recovery phase. Region 1 begins around 5 $\mu A/m^2$ in the growth phase, decreases by about a half to 2.4 $\mu A/m^2$ in expansion, and decreases by a half again to 1.3 $\mu A/m^2$ in recovery. Meanwhile, region 2 starts at 1.3 $\mu A/m^2$, increases very slightly to 1.6 $\mu A/m^2$, and then drops back down to 1.3 $\mu A/m^2$. The increase of region 2 density from the growth phase to expansion phase is a factor of 1.2, which is just a little bit lower than the increase (1.4) of region 2 density from $|AL| < 100\gamma$ to $|AL| \geq 100\gamma$ in the afternoon to midnight sector as reported by *Iijima and Potemra* [1978].

Figure 9 shows region 1 and 2 current layer widths plotted against substorm phase. Variability in the two region 1 growth phase events with respect to their mean is large, so again, the average growth phase region 1 current layer width is less certain than during the other phases. Again, however, region 1 and 2 appear to display different behavior during a substorm. Region 1 width decreases throughout a substorm, while region 2 peaks in width during expansion. Region 1 begins at around 516 km in the growth phase, decreases slightly to 471 km in expansion, and then decreases to 290 km by the recovery phase. Region 2, on the other hand, is at a much narrower width of 135 km during growth, increases to 346 km in expansion and then decreases slightly to 298 km in recovery. These widths seem reasonable since some auroral structures can range from a few kilometer to just over 1000 km in size (such as spirals) [*Davis*, 1979]. Also, current layer widths inferred from Iijima and Potemra's 1978 study indicate widths on the order of hundreds of kilometers. Overall, region 1 current layer width is larger than that of region 2 except for the recovery phase where they are similar.

Figure 10 is a plot of the region 1 and 2 current sheet velocities, normal to the current sheet, versus substorm phase. Region 1 and 2 velocities behave differently during a substorm. The largest region 1 velocity occurs during the growth phase, while the largest region 2 velocity occurs during the expansion phase. Region 1 current sheet velocity begins around -164 m/s in the growth phase, decreases in magnitude to -53 m/s in the expansion phase, and then increases in magnitude very slightly to -65 m/s in recovery. Meanwhile, region 2 velocity is around -63 m/s during growth, increases to -190 m/s during expansion, and then drops back down to -57 m/s in recovery. Interestingly, region 1 decreases and region 2 increases by about the same factor (3.1 and 3.0, respectively) from growth to expansion and then are comparable to each other during recovery. Note also that the velocities of region 1 and 2 current sheets are negative, indicating equatorward or inward motion throughout a substorm. The average magnitude of the current sheet velocities in the ionosphere are on the order of 50-200 m/s. This is comparable to observed auroral velocities. When the equatorward boundary of the auroral oval expands equatorward, it does so at a speed of approximately 150 m/s [see *Nakai et al.*, 1986, Figure 4]. In addition, during a substorm, when auroral arcs near this equatorward boundary begin to disintegrate into "patches," these "patches" drift eastward at speeds of the order 200-300 m/s [*Akasofu*, 1968].

One final result of our study is the perhaps surprising discovery that all of the field-aligned current events determined by *Kelly et al.* [1986] could be associated with a particular substorm phase. None were observed at quiet times. To determine how unique this observation is, we tried to classify the substorm phase of control periods by examining *AE* indices at times exactly one day prior and one day after each event. In doing so, we found that out of the 22 control periods (11 prior and 11 after), there were nine in which no substorms occurred, there were five that did have substorms, there were three with substorms close to but not coincident with the control period, and there were five when no substorm occurred, but high geomagnetic activity was present. Therefore auroral activity as judged from our 22 control intervals, occurs about 45% of the time, and about 25% of the time, we can classify this behavior as substorm like. Thus the fact that all of our events, which are nightside events, are associated with a substorm phase, indicates that substorms play a major role in the generation of the field-aligned currents detected by ISEE 1 and 2.

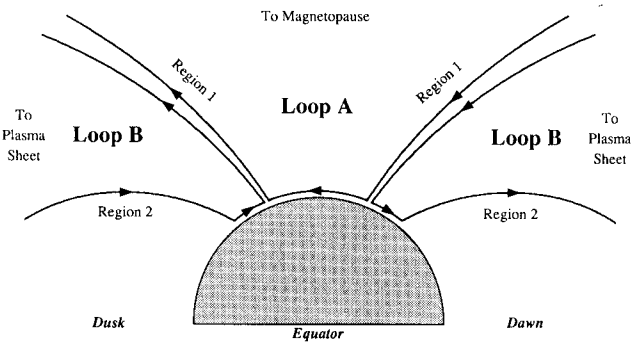

Fig. 11. Schematic diagram illustrating our two-loop model, loops A and B. The view is from the magnetotail looking earthward, with dawn on the right-hand side and dusk on the left. Loop A is poleward of loop B and maps to the magnetopause and is responsive to solar wind applied stresses. Loop B maps to the plasma sheet and is responsive to magnetospheric stresses. Both loops contribute to region 1 currents, but only loop B contributes to region 2.

Discussion

The ISEE 1 and 2 measurements at middle altitudes in the magnetosphere are very consistent with observations obtained at lower altitudes in the ionosphere. When the observed currents are extrapolated to the low altitudes, the current densities and intensities observed during substorms are similar to that seen at low altitudes during disturbed times [*Iijima and Potemra*, 1978]. This consistency indicates that ISEE 1 and 2 are observing the same currents at mid altitudes as Iijima and Potemra studied at low altitudes. While low-altitude spacecraft have not been able to provide observations of current sheet velocities with which to compare the ISEE 1 and 2 data, the ISEE velocity observations are consistent with the velocities of auroral forms which are expected to reflect the motion of current systems. With only one exception in our data set the velocities were inward during all substorm phases.

We have separated our currents into region 1 and region 2 currents as well as by substorm phases, growth, expansion, and recovery. Region 1 currents are defined to be those flowing on or near the polar border of the auroral oval that are down on the dawnside and up on the duskside. The region 2 currents have the operational definition that they are flowing on or near the equatorial boundary of the auroral oval and are up at dawn and down at dusk. These definitions help us identify the spatial location of the current system, but does not necessarily describe the physical context of that current system. It is perhaps better to consider two complete current loops, loop A and loop B as represented in Figure 11, which are driven by the solar wind interaction and magnetospheric stresses, respectively. Loop A would be responsive to the electric potential applied to the magnetosphere, i.e., the merging or reconnection rate. Loop B would be responsive to magnetospheric stresses. Both contribute to region 1 currents, but only loop B contributes to the region 2 current leg. Thus magnetospheric stresses can be monitored by following the rise and fall of the region 2 currents, while the solar wind applied stresses should be proportional to the difference between the region 1 and 2 currents. With this picture in mind, we can interpret the variations seen in region 1 and 2 currents.

Figure 7 shows that region 1 current rises from the growth phase to the expansion phase and then falls. The region 2 current is initially much lower than the region 1 current. It rises from growth to expansion and continues to rise until the two currents are equal in the recovery phase. In our two current loop model the equality of the region 1 and 2 currents during the recovery phase indicate that the solar wind driven system, loop A, has diminished in amplitude. This is in accord with the substorm paradigm in which the recovery phase occurs when the solar wind stress disappears [*Russell and McPherron*, 1973; *McPherron et al.*, 1973]. The increase in region 2 currents from growth to expansion to recovery is also in accord with this model because we expect magnetospheric stresses to accumulate until the solar wind stresses stop. Finally, the increase in region 1 current from growth to expansion appears to be due to the increase in current loop B, the magnetospheric stress loop, rather than loop A, the solar wind stresses. This also is in accord with the substorm model in which recovery is due to the release of the solar wind stress. In this case, growth phase and expansion phase solar wind stresses should be about constant.

The behavior of the current density as a function of substorm phase indicates that the physical processes controlling the two current loops, A and B, may be different. In the case of the region 2 currents which we take to be solely associated with loop B, the magnetospheric stress currents, the current density is constant. This constancy suggests that the current density has reached some upper limit. The total current (or current intensity) can vary in this case by a thickening of the current carrying layer, but the current per unit area is fixed. The temporal variation of the region 1 current implies that the current in loop A is not so limited. During the growth phase the current density appears to be

much greater than the expansion phase. The difference between these two systems may be due to the different sources of the currents or possibly due to differences in the plasmas along the current paths.

The width of the current layer in Figure 9 is not independent of the behavior of the current intensity and density in Figures 7 and 8. The equality of current thickness during the recovery phase is consistent with the disappearance of the loop A contribution to the region 1 current so that region 1 and 2 currents are legs of the same current system. The variation of the region 2 current layer thickness from growth to expansion to recovery may be just the consequence of the apparent upper limit on region 2 current density shown in Figure 8. The reason for the variation in region 1 current layer width seen in Figure 9 is unknown, but this thickness could be constant within the variability exhibited in this Figure. More data are clearly needed here.

A measurement for which we have no low altitude counterpart is the velocity data shown in Figure 10. As illustrated by this figure, the current layers are almost always drifting equatorward. The velocities of these current layers are similar to the velocities of auroral forms, as one might expect. The inward motion is greatest for the region 2 currents during the expansion phase when the inward pressure due to reconnection in the tail might be expected to be the greatest. Otherwise, the velocities are roughly equal. We feel that it is an important observation that only one example of a poleward moving current sheet was found.

It is also important to note that all of our events could be classified according to substorm phase. The currents studied were not selected according to substorm activity. The fact that randomly selected days using the same onset times returned many examples of events at quiet times and during steady geomagnetic activity, indicate that substorms are crucial in the generation of these currents. Region 1 and 2 current systems are integral parts of the coupling of the stresses in the outer magnetosphere with the ionosphere which arise in both dayside and nightside reconnection.

Overall, we note that this study needs to be extended to further events. The results obtained during the expansion and recovery phase seem to be significant when compared to the probable error of the mean as judged from the event to event variation. However, the inferred behavior during the growth phase for each of the region 1 and region 2 currents as well as the region 1 expansion phase current, requires further examples, especially in the region 1 system where the event to event variance is large. We also need to extend this study closer to the midnight region to examine the more complex current systems associated with the Harang discontinuity and the substorm current wedge. Despite the need for further work, however, we feel that these results are sufficiently robust and interesting to be reported and incorporated in our present substorm paradigm.

Conclusions

ISEE 1 and 2 measurements of the region 1 and 2 current at mid altitudes above the nightside auroral oval show that these current systems respond strongly to substorm phase. At quiet times these systems are quite weak, but they increase significantly during the growth, expansion, and recovery phases. Region 1 current intensity peaks in the expansion phase, while region 2 current is at its maximum during the recovery phase. In all phases, region 1 current intensity is equal to or greater than that in region 2. Region 1 current varies from 0.4 to 0.6 A/m during the course of a substorm, while region 2 currents vary from 0.15 to 0.35 A/m, extrapolated to the ionosphere.

The densities of the currents in these regions also vary differently. The region 2 current density remains roughly constant at about 1.4 $\mu A/m^2$, while region 1 currents appear to decrease from about 5 to 1.3 $\mu A/m^2$. The widths of these current sheets also adjust themselves during a substorm. The width of these current systems extrapolated to the ionosphere varies from about 100 to 500 km. Interestingly, the velocity of these sheets is almost always inward towards the equator, at velocities similar to those observed for auroral forms, 50 to 200 m/s.

We interpret these data to be consistent with a model in which these currents flow to couple the outer magnetosphere and the ionosphere in response to the stresses applied by both dayside and nightside reconnection. The region 1 current system is responsive to variations in the stress associated with both dayside and nightside reconnection, whereas the region 2 currents are responsive to only nightside stresses.

Acknowledgments. One of the authors (F. K. Chun) is grateful to the Department of Physics, U. S. Air Force Academy, for their Ph.D. sponsorship and to P. Song for his valuable assistance in the extrapolation of the current sheet velocities. This work was supported by the National Aeronautics and Space Administration under research grant NAG5-1067.

The Editor thanks T. Potemra and M. Sugiura for their assistance in evaluating this paper.

References

Akasofu, S.-I., The development of the auroral substorm, Planet. Space Sci., 12, 273, 1964.

Akasofu, S.-I., Polar and Magnetospheric Substorms, p. 44, D. Reidel, Norwood, Mass, 1968.

Cummings, W. D., R. J. O'Sullivan, and P. J. Coleman, Jr., Standing Alfven waves in the magnetosphere, J. Geophys. Res., 74, 778, 1969.

Davis, T. N., Observed microstructure of auroral forms, in Auroral Processes, edited by C. T. Russell, pp. 171-180, Center for Academic Publications Japan, Tokyo, Japan, 1979.

Davis, T. N., and M. Sugiura, Auroral electrojet activity index AE and its universal time variations, J. Geophys. Res., 71, 785, 1966.

Iijima, T., and T. A. Potemra, The amplitude distribution of field-aligned currents in northern high latitudes observed by TRIAD, J. Geophys. Res., 81, 2165, 1976.

Iijima, T., and T. A. Potemra, Large-scale characteristics of field-aligned currents associated with substorms, J. Geophys. Res., 83, 599, 1978.

Kamei, T., and H. Maeda, Data book 3: Auroral electrojet indices (AE) for January-June 1978, report, World Data Cent. C2 for Geomagn., Kyoto Univ., Kyoto, Jpn., 1981.

Kelly, T. J., C. T. Russell, R. J. Walker, G. K. Parks, and J. T. Gosling, ISEE -1 and -2 observations of Birkeland currents in the Earth's inner magnetosphere, J. Geophys. Res., 91, 6945, 1986.

McPherron, R. L., Growth phase of magnetospheric substorms, J. Geophys. Res., 75, 5592, 1970.

McPherron, R. L., Magnetospheric substorms, Rev. Geophys., 17, 657, 1979.

McPherron, R. L., C. T. Russell, and M. P. Aubry, Satellite studies of magnetospheric substorms on August 15 1968, 9, Phenomenological model for substorms, J. Geophys. Res., 78, 3131, 1973.

Nakai, H., Y. Kamide, D. A. Hardy, and M. S. Gussenhoven, The dynamics of the equatorward boundary of the auroral oval, in Solar Wind-Magnetosphere Coupling, edited by Y. Kamide and J. A. Slavin, pp. 633-641, Terra Scientific, Tokyo, 1986.

Rich, F. J., and M. S. Gussenhoven, The absence of region 1 / region 2 field-aligned currents during prolonged quiet times, Geophys. Res.Lett., 14, 689, 1987.

Russell, C. T., and R. L. McPherron, The magnetotail and substorms, Space Sci. Rev., 15, 205, 1973.

F. K. Chun and C. T. Russell, Institute of Geophysics and Planetary Physics and Department of Earth and Space Sciences, University of California, Los Angeles, CA, 90024.

(Received November 9, 1990;
revised February 19, 1991;
accepted March 25, 1991.)